Effects of layering on the magnetostatic interactions in microstructures of Co_xCu_{1-x}/Cu nanowires

J. De La Torre Medina, M. Darques, T. Blon, and L. Piraux
Unité de Physico-Chimie et de Physique des Matériaux, Université Catholique de Louvain, Place Croix du Sud 1, B-1340 Louvain-la-Neuve, Belgium

A. Encinas
Instituto de Física, Universidad Autónoma de San Luis Potosí, Avenida Manuel Nava 6, Zona Universitaria, 78290 San Luis Potosí, SLP, Mexico

(Received 25 June 2007; revised manuscript received 12 October 2007; published 14 January 2008)

Arrays of electrodeposited CoCu/Cu multilayered nanowires have been characterized by ferromagnetic resonance and magnetometry measurements in order to study the effect of the dipolar interactions on the effective anisotropy field as a function of the magnetic and nonmagnetic layer thicknesses. Breaking the continuous cylinder geometry results in a reduction of the effective anisotropy field, which can be modified over a large range of values starting from 7 kOe in the case of nonlayered continuous nanowires down to nearly zero for the thinnest magnetic layers. An analytical model is presented to describe the magnetostatic interactions between magnetic layers and their effect on the total anisotropy field which shows a very good agreement with the experiments. Moreover, the model allows generalizing the description of the effective magnetostatic field as a function of the aspect ratio of both the magnetic and the nonmagnetic layers for multilayered nanowires of any combination of materials. A general anisotropy diagram is presented that describes the geometrical conditions required to obtain an easy axis parallel or perpendicular to the wire axis, thus providing a guide for the engineering and fine-tuning of the magnetic properties of these systems.

DOI: 10.1103/PhysRevB.77.014417 PACS number(s): 75.30.Gw, 75.60.Ej, 76.50.+g

I. INTRODUCTION

Multilayered magnetic heterostructures have been widely studied for almost 20 years since the discovery of the giant magnetoresistance (GMR) effect.[1] Multilayered magnetic nanowires appeared as an invaluable tool to study GMR effects in the current perpendicular to the plane configuration.[2] Since their introduction in 1994,[3,4] arrays of multilayered nanowires have been fabricated by potential modulated single bath electrodeposition combining a wide variety of materials such as Co/Cu,[5–10] NiFe/Cu,[4,11] Fe/Cu,[12] Co/Au,[13] NiCo/Cu,[14,15] Ni/Pt,[16] Ni/Cu,[17] CoFe/Cu,[18] CoPt/Pt,[19] and CoFeNi/Cu.[20]

Most GMR studies were done on multilayers formed by a large number of ferromagnetic/nonferromagnetic (FM/NM) layers, nevertheless, recent developments in both micro-/nanolithography and measuring techniques have made it feasible to perform two- and four-probe MR measurements in single nanowires[21–23] and, as shown more recently, in single very short cylindrical wires containing a very small number of layers.[24] This has launched great interest in using these geometrically simple structures to study spin polarized effects such as electrical spin injection,[25] domain wall MR,[26,27] magnetic field sensors,[28] and spin dependent thermoelectric effects.[29]

These results have stressed the need to reconsider the methods and techniques used to grow these multilayered nanowires. In particular, the overall magnetic properties of these structures will depend sensibly on the specific magnetic properties of each of the different magnetic layers of the system, such as their coercive or switching fields, saturation fields, magnetic anisotropies, and different coupling mechanisms that might occur among the layers and among the wires.

In this sense, significant advancements have been achieved in these type of multilayered structures. For instance, Chen *et al.* have shown using Ni/Cu multilayered nanowires, that the effective anisotropy can be controlled over a wide range of values by adjusting the layer thickness and the corresponding shape anisotropy of the magnetic layers.[17] Moreover, several studies have underlined the role of the magnetostatic coupling as a function of the geometrical parameters of the system.[30] More recently, it has been shown that in the case of Co/Cu multilayers, the crystallographic structure of the CoCu layers can be controlled by deposition parameters such as the *p*H of the electrolyte and the applied voltage.[31] Indeed, by proper adjustment of these parameters, the CoCu magnetic layer can be obtained as a fcc type, with no magnetocrystalline anisotropy, or with a hcp structure in which the orientation of the *c* axis can be fixed either parallel or perpendicular to the wire axis, introducing an important magnetocrystalline anisotropy contribution.[31]

Despite these advancements, control of the microstructure in order to modify the magnetic properties seems restricted to noncubic materials such as Co and Pt based alloys (CoPt, FePt). This is due to the fact that cubic materials (Ni, CoFe, CoNi, NiFe) have lower magnetocrystalline anisotropy constants, which are often negligible because of the tendency of obtaining polycrystalline layers when using electrodeposition.

Under these conditions, control of the magnetic properties depends entirely on magnetostatic effects, specifically, the shape anisotropy and dipolar coupling mechanisms. As

shown by Sun *et al.*, the shape anisotropy can be controlled as a function of the magnetic layer thickness, which defines the aspect ratio.[32] At high aspect ratio, the magnetic layers behave like cylindrical rods with their easy axis along the cylinder axis, while at low aspect ratio, cylindrical disks are obtained, which favor an easy magnetization direction perpendicular to the cylinder axis. However, this behavior is also influenced by the magnetostatic coupling between the magnetic layers, which depends on the thickness of the nonmagnetic layer.[33,34] Indeed, for large spacer layer thickness, the magnetic layers are almost decoupled and behave as isolated magnetic units, while at lower separation, the dipolar coupling between layers tends to lower the rate at which the magnetic layer aspect ratio forces the easy axis transition from parallel to perpendicular to the cylinder axis. These studies have been based on the measurement of hysteresis loops or GMR cycles, and the magnetic properties have been analyzed qualitatively based on parameters such as coercive field, remanence, and saturation field.

A more detailed analysis of the effect of layering on the magnetic anisotropy is needed to gain a better understanding of the dipolar interactions within the entire system. In the present study, CoCu/Cu multilayers are considered. In particular, the case of fcc-like magnetic layers are used in order to avoid magnetocrystalline contributions.[31] Furthermore, low density arrays are used to minimize the interwire interactions. The effect of layering is considered as a function of the magnetic layer thickness for series of samples having different nonmagnetic layer thicknesses. An analytical magnetostatic model is proposed in order to consider both the effect of the magnetic layer thickness and the dipolar coupling between layers, which is complemented by ferromagnetic resonance measurements that allow an accurate determination of the effective anisotropy field. The measured variation of the effective anisotropy field shows a very good agreement with the model, which can predict both the effect of the magnetic layer aspect ratio and the spacer layer thickness within the validity of the approximations used. Moreover, the model allows generalizing the description of the effective magnetostatic field as a function of the aspect ratio of both the magnetic and the nonmagnetic layers for multilayered nanowires of any combination of magnetic and nonmagnetic materials. From this generalization, a general anisotropy diagram is presented that describes the geometrical conditions required to obtain an easy axis parallel or perpendicular to the wire axis, thus providing a guide for the engineering and fine-tuning of the magnetic properties of these systems.

II. EXPERIMENTAL SETUP

Arrays of multilayered $Co_{0.96}Cu_{0.04}$/Cu nanowires have been fabricated by standard three-probe electrodeposition into the pores (140 nm in diameter) of 21 μm thick track-etched polycarbonate membranes produced at the laboratory scale. Owing to the improved properties of these membranes, the electrodeposited nanowires are almost perfectly cylindrical, parallel (deviation is less than 5°), and present a very low surface roughness.[35]

In order to ensure a low magnetostatic coupling between nanowires, a low porosity membrane (4%) was used. A Cr(20 nm)/Au(600 nm) layer was evaporated on one side of the membrane to serve as a cathode for the electrodeposition. Multilayered nanowires have been grown at room temperature using the so-called single bath technique. The composition of the electrolyte was 238.5 g/l $CoSO_4$ +0.75 g/l $CuSO_4$+30 g/l H_3BO_3. In order to assure that the $Co_{0.96}Cu_{0.04}$ layers have no magnetocrystalline anisotropy, the *p*H was lowered down to 2.0 by adding concentrated H_2SO_4.[31] The potential, measured vs a Ag/AgCl reference electrode, is alternatively switched between −0.95 V to deposit CoCu and −0.5 V for Cu. Additionally, continuous, nonlayered reference samples of the $Co_{0.96}Cu_{0.04}$ alloy were grown under a constant reduction potential of −0.95 V. Finally, pure Co nonlayered samples have also been prepared using a 238.5 g/l $CoSO_4$+30 g/l H_3BO_3 electrolyte with the *p*H adjusted to 2.0, under a constant potential of −0.95 V.

For this study, two series of multilayered samples having a diameter of 140 nm were fabricated in which the thickness of the CoCu magnetic layers was varied between 17 and 213 nm. In one series, the copper layer thickness was kept at constant value of 4 nm, while on the second series, the Cu thickness was 20 nm. A statistical analysis using transmission electron microscopy (TEM) imaging was carried out over an extensive number of isolated nanowires from different samples in order to estimate the average layers' thickness and their dispersion. The extraction of the nanowires from the membrane is done by dissolving the membrane using hot dichloromethane (CH_2Cl_2), then removing the gold cathode with KI. Dichloromethane nanowire droplets are then spread onto a grid for TEM observation.

Ferromagnetic resonance (FMR) measurements were carried out at room temperature using a microstrip transmission line technique. The stripline was fabricated by evaporation of a Cr(20 nm)/Au(100 nm)/Cu(800 nm)/Au(200 nm) layer through a 150 μm wide metallic mask on the free membrane surface. A typical FMR spectrum is obtained by sweeping the magnetic field applied parallel to the nanowires, from saturation (10 kOe) down to zero at a given constant excitation frequency. These measurements are then repeated at different frequencies up to 50 GHz to obtain the dispersion relation from which the different contributions to the effective anisotropy field can be extracted.

Hysteresis loop measurements were performed at room temperature using an alternating gradient magnetometer (AGM). The magnetic field was applied in the directions parallel and perpendicular to the nanowire's axis and swept between ±10 kOe.

III. MODEL

In order to gain a more detailed understanding of the effects of the magnetic interactions in an array of multilayered nanowires, an analytical model that depends on geometric parameters and demagnetizing factors for cylinders is proposed. First, the simple case of an array of nonlayered magnetic nanowires having no magnetocrystalline anisotropy

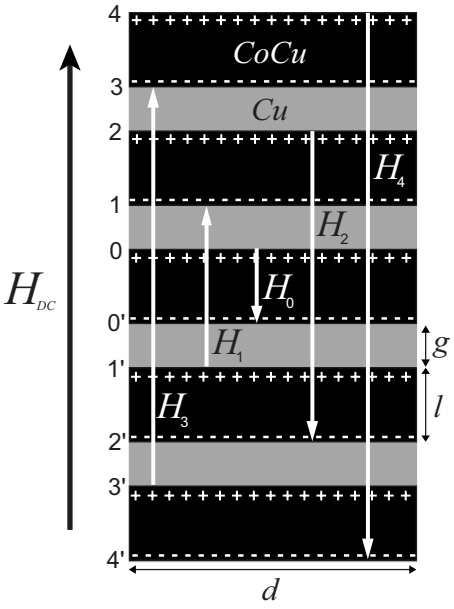

FIG. 1. Lateral sketch of a multilayered nanowire with diameter d. The cobalt and copper layer of thickness are l and g, respectively. The demagnetizing fields H_n appear as a result of the polarization of the magnetic layers under biasing by magnetic field H_{DC}.

contribution is considered, and the multilayered case will be treated subsequently.

At room temperature, the main contributions to the effective field of an array of magnetic nanowires are the magnetocrystalline and the shape anisotropies.[36,37] When the magnetocrystalline anisotropy contributions are negligible, the effective field is purely magnetostatic, and it can be written in terms of the self-demagnetizing field for an isolated infinite cylinder with a saturation magnetization M_s and the dipolar interactions between wires in the following form:[36]

$$H_{eff} = 2\pi M_s(1 - 3P), \tag{1}$$

where P is the porosity or filling factor, defined as the product of the areal pore density by the pore surface. As seen below, this expression provides an upper bound to the value of the total magnetostatic field once the continuous wires are segmented to form a multilayered system.

In the case of an array of multilayered nanowires magnetically saturated parallel to their axis, other dipolar interactions appear as a result of the creation of a larger number of interfaces, as shown schematically in Fig. 1. In principle, each magnetic layer will interact with other magnetic layers of the same wire as well as with those of neighboring wires. To simplify the model, the following is limited to low density (low porosity) arrays of multilayered nanowires, so that the layer to layer interaction is considered only between layers in the same wire separated by nonmagnetic layers of thickness g, which is considered smaller than the interwire separation l_w. Moreover, under the action of a magnetic field applied parallel to the wire axis, this approximation seems reasonable since dipolar interactions between magnetic layers from different wires are minimized when the wires are saturated along the cylinder axis. Finally, as mentioned previously, the magnetocrystalline anisotropy contribution in the magnetic layers will be neglected.

Rewriting the shape anisotropy field of a single continuous isolated cylinder with a diameter d and length l, as a function of the demagnetizing factors in the directions parallel ($N_{\parallel}^{cyl}$) and perpendicular ($N_{\perp}^{cyl}$) to the axis of the cylinder and using the expression $2N_{\perp}^{cyl}+N_{\parallel}^{cyl}=1$ (in *System International*), the effective magnetostatic field is expressed as follows:

$$H_{eff}^{cyl} = 4\pi M_s(N_{\perp}^{cyl} - N_{\parallel}^{cyl}) = 2\pi M_s(1 - 3N_{\parallel}^{cyl}), \tag{2}$$

where $N_{\perp}^{cyl}$ and $N_{\parallel}^{cyl}$ are the demagnetizing factors in the directions perpendicular and parallel to the axis of the cylinder. The demagnetizing factor $N_{\parallel}^{cyl}$ can be expressed as the ratio of the average demagnetizing field to the average magnetization of the entire sample.[38] This definition corresponds to the magnetometric demagnetizing factor developed by Brown,[39] where a uniform magnetized cylinder is modeled as a solenoid. The formula for the magnetometric demagnetizing factor

$$N = 1 - \frac{4}{3\pi r}\{\sqrt{1+r^2}[r^2K(k_s) + (1-r^2)E(k_s)] - 1\}, \tag{3}$$

is an exact analytical expression for a cylinder with the dimensions given as before,[40] where $K(k_s)$ and $E(k_s)$ are the complete elliptical integrals of the first and second kinds of modulus $k_s = 1/\sqrt{1+r^2}$ being $r=l/d$ the aspect ratio of the cylinder.

Let us now consider an isolated multilayered wire of diameter d with magnetic and nonmagnetic layers of thickness l and g, respectively, as shown in Fig. 1. The total demagnetizing field along its axial direction is the sum of subfields created at the internal layers interfaces, which are taken into account using the scheme proposed by Pant.[41] That is, consider the central magnetic layer with its corresponding interfaces, labeled 0 and $0'$ and magnetostatic field H_0. As the number of layers is increased, so is the number of interfaces, their effect on the total magnetostatic energy of the central element can be described considering the fields generated from the pair interaction among sequentially ordered interfaces. This is illustrated in Fig. 1, in which a magnetostatic field H_i is considered for each pair of interfaces, i and i'. As seen in this figure, as more layers are considered, the corresponding stray field is lower in magnitude with direction opposite to the previous one.

In the case of an isolated multilayered nanowire with a large and finite number n of magnetic layers, the dipolar interactions along the direction of the wire axis can be expressed as a finite monotone alternating sum of demagnetizing fields H_i, in analogy with the analysis developed by Pant for rectangular slabs.[41] Therefore, the total demagnetizing factor in this direction $N_{\parallel}$ is also expressed as an alternating sum of demagnetizing factors N_i, which correspond to each demagnetizing field H_i:

$$N_{\parallel} = \left| \sum_{i=0}^{n} (-1)^i N_i \right| = \left| \sum_{k=0}^{j} (N_{2k} - N_{2k+1}) \right|, \quad (4)$$

where $j=(n-1)/2$. The two possible orientations of the external magnetic field along the wire axis are comprised in the absolute value in Eq. (4). The ith demagnetizing factor N_i is given by Eq. (3), in which, for convenience, the aspect ratio r is replaced by a value that depends on i:

$$r_i = \begin{cases} (2k+1)r_l + 2kr_g & \text{if } i = 2k \\ (2k+1)r_l + 2(k+1)r_g & \text{if } i = 2k+1, \end{cases} \quad (5)$$

where $k=0,1,2,\ldots,j$ and $r_l=l/d$ and $r_g=g/d$ are the aspect ratios of the magnetic and the nonmagnetic layers. Let us suppose that the isolated multilayered wire behaves magnetically in the same way as the isolated continuous cylinder does. Under this assumption, the effective field of the multilayered wire is represented by the right hand side of Eq. (2), where in this case, the demagnetizing factor $N_{\parallel}$ is calculated by Eq. (4).

However, in practice, measurements are performed on arrays of nanowires and not on single wires, so the effective dipolar interaction between them has to be taken into account. In the limit $l_w \gg g$, the dipolar field experienced in a single multilayered wire from the whole array can be regarded as a dipolar field generated by an array of nonlayered wires. In other words, the effective anisotropy field for an array of multilayered nanowires $H_{eff}^{\mathrm{Co/Cu}}$ must be weighted only by multiplying the demagnetizing field of an isolated multilayered wire by the factor $1-3P$, in analogy with the case of an array of nonlayered wires.[36] As a result, the effective field for an array of multilayered nanowires is given as follows:

$$H_{eff}^{\mathrm{Co/Cu}} = 2\pi M_s (1-3P)\left(1 - 3\left|\sum_{k=0}^{j} (N_{2k} - N_{2k+1})\right|\right), \quad (6)$$

where the coefficient has been taken as in Eq. (1), which is the reference value of the continuous infinite wire embedded in an array with packing fraction P. Equations for the demagnetizing factor (3), the modulus k_s, and the magnetic and the nonmagnetic aspect ratios r_l and r_g are considered in the whole calculation. This expression contains two factors: the first one corresponds to the effective magnetostatic field of a single infinitely long continuous wire which interacts with the rest of the wires in the array, Eq. (1); the second factor takes into account the additional magnetostatic effects that result once the wire is segmented into smaller magnetic units to form the multilayer.

Finally, this effective field ($H_{eff}^{\mathrm{Co/Cu}}$) can be determined experimentally by ferromagnetic resonance using the dispersion relation obtained, with the magnetic field applied parallel to the wires, by performing a linear fit to the resonance condition,

$$\frac{f}{\gamma} = H_r + H_{eff}^{\mathrm{Co/Cu}}. \quad (7)$$

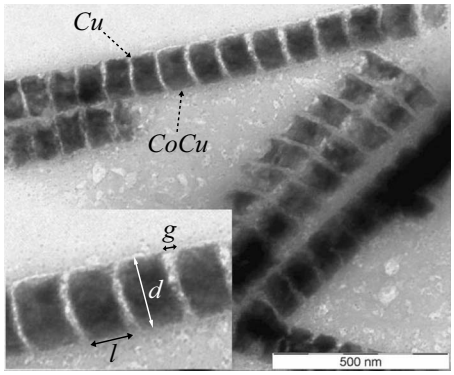

FIG. 2. TEM image for 140 nm CoCu/Cu nanowires electrodeposited using a *p*H 2 electrolyte. The inset shows a detail of the nanowires and their geometrical parameters.

In the above equation, γ is the gyromagnetic ratio (3.05 GHz kOe^{-1} for Co) and H_r the resonance field measured at the given excitation frequency f.

IV. RESULTS AND DISCUSSION

Before considering the case of an array of CoCu/Cu multilayered nanowires, FMR was used to measure an array of continuous CoCu nanowires in order to quantify parameters such as the saturation magnetization of the alloy and the effective field which will serve as reference values. For this purpose, an array of nonlayered CoCu nanowires has been grown and measured using ferromagnetic resonance. The values of M_s and $H_{eff}^{\mathrm{Co/Cu}}$ determined with the field applied parallel to the wires were 1172 emu/cm^3 and 6.84 kOe, respectively. This value of M_s is 14% smaller than for pure cobalt (1370 emu/cm^3) and it will be considered the same for all the multilayered samples fabricated from the above solution. Using these experimental parameters and Eq. (6), the changes of the effective anisotropy field with layering will be calculated and compared with the experiment.

A. Influence of layering

Figure 2 shows a TEM image of a segment of a multilayered wire where the geometrical parameters l, g, and d are indicated in the inset. Since the actual layer dimensions are not fully constant due to fluctuations of the amount of deposited materials during electrodeposition, a wide statistical analysis of these parameters was carried out over a considerable number of segmented wires. Hereafter, the quoted values for the thickness of both magnetic and nonmagnetic layers correspond to the average thickness determined by TEM.

It is well established that the magnetic properties of an array of multilayered nanowires can be tailored with the magnetic and nonmagnetic layer thicknesses.[17,30,33] Several authors have pointed out the role played by the changes in the shape anisotropy contribution as a function of the thickness of the magnetic layer, and the dipolar coupling between layers as a function of the spacer layer thickness.

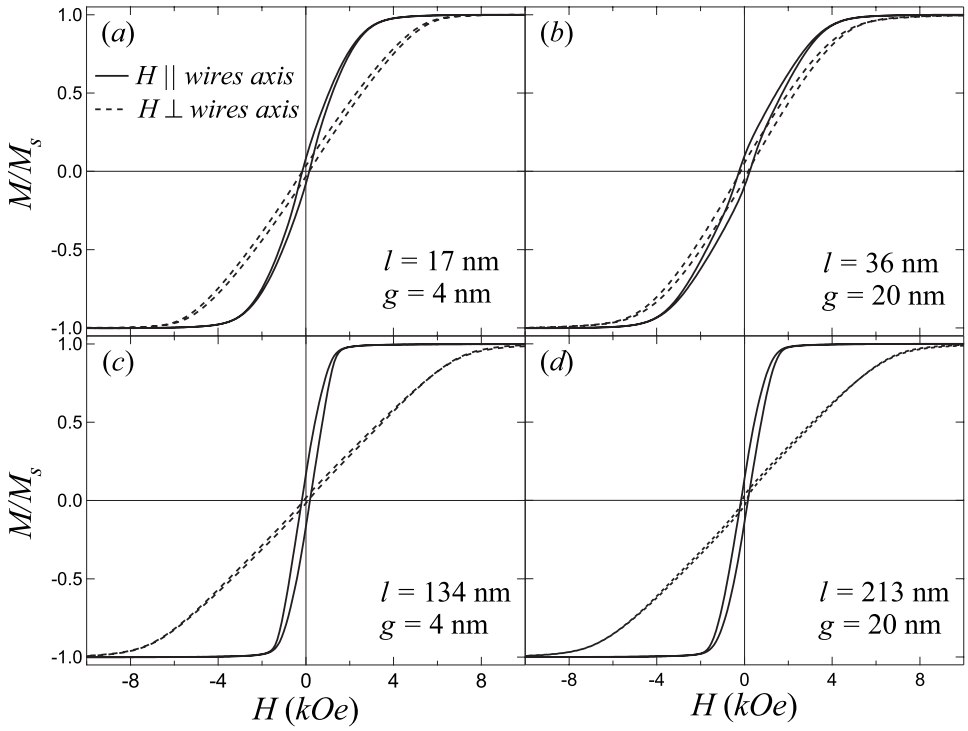

FIG. 3. Hysteresis loops measured with the external field applied parallel and perpendicular to the wire axis for multilayered CoCu/Cu nanowires with different copper and cobalt layer thicknesses: (a) CoCu(17 nm)/Cu(4 nm), (b) CoCu(36 nm)/Cu(20 nm), (c) CoCu(134 nm)/Cu(4 nm), and (d) CoCu(213 nm)/Cu(20 nm).

In order to evidence the variation of the magnetic properties of arrays of CoCu/Cu nanowires with the layering, hysteresis loops for the two series of samples were measured, with the magnetic field applied parallel and perpendicular to the wires axis. Two samples from each series (g=4 and 20 nm) were considered. The samples were chosen such that, for the first series (g=4 nm) l were 17 and 134 nm and for the second one (g=20 nm) l were 36 and 213 nm, which correspond to the shortest and largest magnetic layers thicknesses in each series of samples.

As can be seen from the normalized hysteresis loops shown in Fig. 3, the magnetic properties of the nanowires' arrays are strongly affected with layering and particularly, with the magnetic layer thickness. Comparing between the thinnest and the thickest magnetic layers in each series, Figs. 3(a) and 3(c), or 3(b) and 3(d), it can be seen that the magnetic anisotropy is significantly reduced when the magnetic layer thickness is reduced. In particular, when the field H is applied parallel to the wires, the magnetic saturation is reached at lower fields for the thicker magnetic layers and it increases as thickness is decreased. For the first series (g =4 nm), the saturation field $H_s^{\parallel}$ for this direction decreases from 5 to 2.7 kOe when l increases from 17 to 134 nm. For the second series (g=20 nm), $H_s^{\parallel}$ decreases from 6.5 to 3.3 kOe when l increases from 36 to 213 nm.

Inversely, when the magnetic field is applied along the direction perpendicular to the wires axis, the saturation state is reached at lower fields in the samples with the thinner magnetic layers. That is, in this applied field direction, the saturation field $H_s^{\perp}$ is about 7.5 and 9 kOe for samples with smaller l values corresponding to the first and second series of samples, respectively, whereas for the thicker magnetic layers, the saturation field $H_s^{\perp}$ remains near 10 kOe. Thus, the easy magnetization direction along the wires axis is reinforced for larger magnetic layers. Conversely, thinner magnetic layers favor the direction perpendicular to the wires axis as an easy magnetization direction.

In order to have an accurate determination of the effective field, the FMR properties of these multilayers have been measured. Figure 4(a) presents a set of transmission spectra recorded at 34 GHz for both reference samples, that is, continuous Co and CoCu nanowires and three multilayered samples with a spacer layer thickness of 4 nm and different magnetic layer thickness, while Fig. 4(a) shows their corresponding dispersion relations, where the straight lines correspond to the fit of the experimental data to Eq. (7).

From the spectra shown in Fig. 4(a), it can be observed that at the same frequency, the multilayered samples present higher resonance fields than the reference samples. In particular, the shift of the resonance field increases as the magnetic layer thickness decreases. In this case, the highest resonance field (8 kOe) is measured on the CoCu(17 nm)/Cu(4 nm) sample, which represents a change of 3 kOe with respect to the effective field of the reference CoCu sample.

From Eq. (7), it can be seen that at a given frequency, an increase of the resonance field corresponds to a decrease of the effective anisotropy field, suggesting that the effective anisotropy of the wires is lowered once the wires are segmented to form a multilayer, and decreases as the magnetic layer thickness is further reduced. This can clearly be seen in

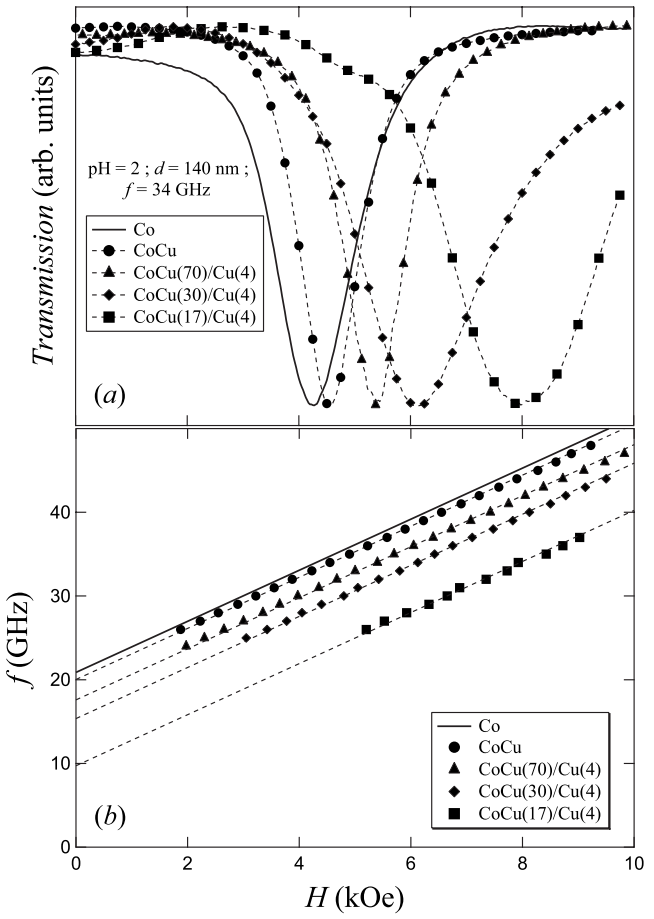

FIG. 4. (a) Transmission spectra recorded at 34 GHz and (b) the corresponding dispersion relation for each sample for arrays of nonlayered and multilayered nanowires electrodeposited at pH=2. The type of sample and values for the layers thickness in nm are indicated in the figure.

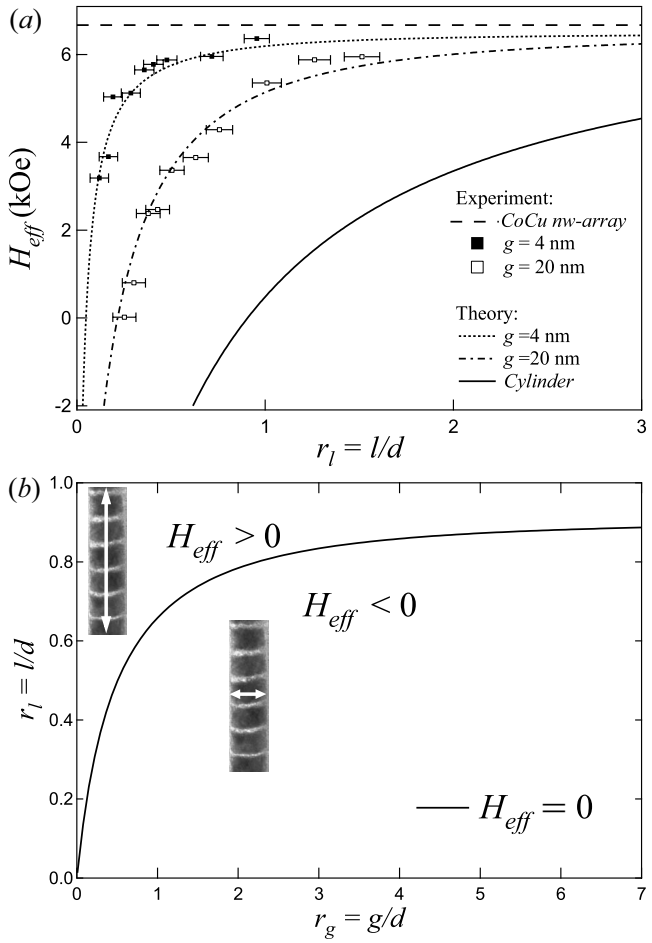

FIG. 5. (a) Anisotropy field as a function of the magnetic layer aspect ratio r_l for arrays of multilayered CoCu/Cu nanowires. The two series of samples are compared corresponding to the magnetic interlayer separation g=4 nm and g=20 nm. Experimental data for each series of samples are fitted with the analytical model given by Eq. (6). (b) Anisotropy diagram as a function of the aspect ratios of the magnetic $r_l=l/d$ and the nonmagnetic $r_g=g/d$ layers. The continuous line shows the values of r_l and r_g for which the effective anisotropy is zero. Above this curve, the effective field is positive, while below it is negative. The magnetization easy axis is represented by the white arrow.

Fig. 4(b) from the measured dispersion relations. From this figure, it can be noticed that the shift of the dispersion relation is not constant with the magnetic layer thickness l, but rather asymptotic, up to the resonance field corresponding to the nonlayered CoCu nanowires array (circles). Thus, for a constant spacer layer thickness, the effective field for multilayered CoCu/Cu nanowires increases with the magnetic layer thickness up to the value of the CoCu sample.

B. Validity of the model

The variation of the effective field with the magnetic and the nonmagnetic layer thickness was analyzed in terms of the effective anisotropy field determined by FMR for the two series of samples with magnetic layer thickness l varying in the range from 17 up to 213 nm for two constant spacer layer thicknesses g (4 and 20 nm).

The effective field as a function of the magnetic layer aspect ratio $r_l=l/d$, for both series of samples, is shown in Fig. 5(a). From this figure, we can see an increase of the effective field approaching a constant limiting field H_{lim} =6.5 kOe as the aspect ratio increases. This limiting value corresponds to the effective field for an array of nonlayered CoCu nanowires (horizontal dashed line at the top of the figure). On the other hand, as the aspect ratio is lowered, the effective field decreases. Notice that the departure from the upper limit takes place at different aspect ratios, depending on the thickness of the nonmagnetic layer. Moreover, as mentioned above, the effective field is always positive (favoring an easy axis parallel to the wires) and only the Co/Cu multilayered sample with l=36 nm and g=20 nm has an effective field close to zero, showing a nearly isotropic behavior as observed from its corresponding hysteresis loop in Fig. 3(b). From the results shown in this figure, the effect of the nonmagnetic layer thickness on the dipolar interaction and the effective magnetostatic field can be evidenced. Indeed, it can be noticed that although H_{eff} increases with the magnetic layer aspect ratio r_l for both series of samples, the limiting

value H_{lim} is reached at lower aspect ratios for the series with thinner copper layers ($g=4$ nm). Moreover, for a given aspect ratio, the effective field is lower for the multilayers having a thicker spacer layer. These differences in the effective field are attributed to the dipolar interaction between the magnetic layers which depends on the spacer layer thickness.

In order to give a more detailed insight of the effective field behavior and dependence on the interlayer dipolar coupling, the effective field given by Eq. (6) has been calculated and compared to the experimental data for the two series of samples, as shown in Fig. 5(a). This calculation is done using the effective field of the nonlayered CoCu sample measured by FMR and the average spacer layer thickness measured by TEM. For reference, the effective shape anisotropy field of a single isolated cylinder as a function of the aspect ratio is also plotted (continuous line). As can be seen from the figure, the model describes with excellent agreement and remarkable accuracy the behavior observed from the experimental data within the range of aspect ratios considered. Moreover, this figure allows a direct interpretation of the effect of the spacer layer thickness in the interlayer coupling and the effective magnetostatic field.

First, let us recall that the effective field is considered to be purely magnetostatic, that is, magnetocrystalline anisotropy contributions are neglected. Furthermore, the magnetostatic interactions between layers in different wires are also neglected. Under these conditions, the effective field of a multilayered nanowire results from the combination of the shape anisotropy of the magnetic layers and the dipolar interaction between them. In order to understand how this effect contributes to the effective magnetostatic field, consider first the limiting case of noninteracting magnetic layers, that is, $g \gg l$. The effective, or total, anisotropy field is given only by the shape anisotropy of the magnetic layers which corresponds to that of an isolated cylindrical rod with an aspect ratio r_l. The shape anisotropy of an isolated magnetic cylinder as a function of the aspect ratio is well known,[39] and corresponds to the continuous line shown in Fig. 5(a), which has been calculated using Eqs. (2) and (3). At high aspect ratios, $r_l=l/d \geqslant 10$, the cylinder is considered infinite, and the value of the shape anisotropy converges to an upper limit given by Eq. (1). This upper bound is shown as a horizontal dotted line in Fig. 5(a). As the aspect ratio decreases, so does the shape anisotropy, the system becomes isotropic at a critical aspect ratio value of $r_l=0.906$. Above this critical value, the system corresponds to a cylindrical rod and favors an easy axis parallel to the cylinder axis, whereas for $r_l < 0.906$, the systems correspond to a cylindrical disk and the easy axis is perpendicular to the cylinder axis.[39,42]

Upon reducing the spacer layer thickness, the interaction between layers increases and the effective field can no longer be considered as that of an isolated cylinder. The variation of the effective field with the magnetic layer aspect ratio should depart from that of the isolated cylinder. This is seen from the results shown in Fig. 5(a), which suggest that for a given spacer layer thickness, $H_{eff}^{Co/Cu}$ varies as a function of the aspect ratio according to Eq. (6). The curve describing this variation for a given spacer layer thickness lies between the limit of the isolated cylinder (continuous line) and the continuous and infinite wire (horizontal dotted line). In particular, as the spacer layer thickness becomes smaller, the function describing the effective field will move toward the limit of the infinite continuous wire. For a given magnetic layer thickness, or aspect ratio, the effective field will be higher as the spacer layer thickness is decreased and in consequence, the reduction of the effective field will shift toward lower values of r_l, as seen in Fig. 5(a). These results are consistent with those reported for NiCo/Cu[30] and Ni/Cu[32] multilayered nanowires.

From the schematics shown in Fig. 1, it can be seen that the effect of the dipolar interaction is to reduce the demagnetizing field of an individual layer favoring a head-to-tail alignment of the magnetization between adjacent layers. That is, dipolar interactions tend to move the boundary between the rod-shaped segments and the disk-shaped segments to lower magnetic aspect ratios.[30,32] Physically, the shift of this boundary is equivalent to stretching the magnetic segments as if they had a larger aspect ratio.

The model provides very good agreement and an accurate description of the behavior of the effective field as a function of the main geometrical parameters of the multilayered system. As mentioned before, a main issue regarding these types of magnetic systems is the possibility to tailor and control their magnetic properties. Equation (6) describing the effective field is expressed as the product of two terms. The first one is given in terms of the saturation magnetization of the magnetic material, the wire packing fraction, and that corresponds to limit of the homogeneous nonlayered array of nanowires. The second term depends on the wire diameter and both the magnetic and the nonmagnetic layer aspect ratios. On observing the results presented in Fig. 5(a), it is clear that for a given spacer layer thickness the effective field will go through zero at a given magnetic layer aspect ratio. Inversely, for a given aspect ratio of the magnetic layers, it should be possible to find the spacer layer thickness at which the effective field will be zero. In other words, it is possible to determine the geometrical conditions needed to obtain multilayered nanowires with an effective field, which favors an easy axis parallel or perpendicular to the wire axis, and even the case of an isotropic nanowire, which can serve as a design guide in order to tailor specific magnetic properties. For this purpose, the geometrical conditions needed for the effective field to be zero have been calculated in the general case of a multilayered cylindrical wire. This is done from Eqs. (3), (5), and (6), where it can be seen that the zeros of the effective field are determined as a function of only the dimensionless parameters corresponding to the aspect ratios of both the magnetic (r_l) and the nonmagnetic (r_g) layers. Figure 5(b) shows the anisotropy diagram for a single multilayered nanowire. The continuous line represents the set of aspect ratios of both magnetic and nonmagnetic layers, for which the effective magnetostatic field is zero, and defines the regions, for which the magnetostatic anisotropy favors an easy axis parallel ($H_{eff}>0$) or perpendicular ($H_{eff}<0$) to the cylinder axis.

This diagram shows that in the limit of thick nonmagnetic layers, the magnetic layers are decoupled and the rotation of the easy axis from the direction parallel or perpendicular to the cylinder axis can only take place below a critical aspect ratio value of $r_l=0.906$, which is the one predicted for a

single magnetic metal cylinder. As expected, above this critical value, the easy axis is parallel to the wires, whereas below this value, the magnetic layers are in the cylindrical disk regime and favor an easy axis perpendicular to the cylinder axis. As the spacer aspect ratio is reduced, the interlayer coupling increases and the easy axis transition takes place at lower magnetic aspect ratio values. Since the dipolar interaction moves the boundary where the isotropic point is obtained, the aspect ratio r_l at which the easy axis rotation takes place decreases as the aspect ratio r_g decreases.

In other words, the diagram describes how the boundary between the rod-shaped segments and the disk-shaped segments moves to lower magnetic layer aspect ratios as a function of the spacer layer aspect ratio. The critical value at which the system becomes isotropic, $H_{eff}=0$, describes how much the magnetic layer aspect ratio needs to be reduced so that for a given thickness of the nonmagnetic layer, the transition boundary is equal to that of the isotropic isolated cylinder (0.906).

Finally, it is worth mentioning that this diagram is general and valid for a single multilayered nanowire that alternates a magnetic and a nonmagnetic layer, for whatever combination of materials. Indeed, the existence of the isotropic point and the possibility to induce a rotation of the easy axis is purely geometrical and, as seen from Eq. (6), depends only on the aspect ratio of both the magnetic and nonmagnetic layers. As mentioned before, this description is limited to the case in which the effective anisotropy field of an array of multilayered nanowires is purely magnetostatic, and for wire densities in which the dipolar interaction between layers in neighboring wires can be neglected.

In this sense, detailed studies of dipolar interactions in multilayered Ni/Cu nanowires have been reported and compared with micromagnetic simulations.[17,32–34] In particular, these systems are purely magetostatic and have a relatively low porosity. The isotropic point has been observed at magnetic layer aspect ratio very close to unity when the nonmagnetic layer is thick. On the other hand, the structures with a magnetic easy axis perpendicular to the wires have magnetic and nonmagnetic layer aspect ratios which are consistent and in good agreement with the diagram in Fig. 5(b), namely, $r_l=r_g=0.1$. Other recent studies of the effects of the interlayer interaction include both Co/Cu and CoNi/Cu multilayered wires grown in anodized alumina templates.[15,30] Unfortunately, these templates have a much higher porosity, which hinders a direct comparison with our results. Moreover, as pointed out by the authors, magnetocrystalline anisotropy contributions cannot be overruled. However, in NiCo/Cu multilayers, the isotropic point is obtained at a magnetic layer aspect ratio of 0.2, when the nonmagnetic layer aspect ratio is 0.014, which is consistent with the results in Fig. 5(b), reflecting the need of very thin magnetic layers when the dipolar interaction is strong (thin spacer layers).

V. CONCLUSIONS

The influence of the layering on the dipolar interactions in arrays of electrodeposited multilayered CoCu/Cu nanowires has been studied as a function of the magnetic layer thickness for several spacer layer thicknesses. Both FMR and AGM measurements have shown that the reduction of the CoCu layer thickness as well as the increase of the Cu spacer layer thickness lead to a reduction of the effective anisotropy field. An analytical magnetostatic model has been proposed which takes into account the shape anisotropy and dipolar interactions in order to describe the behavior of multilayered nanowire arrays as a function of the main geometrical parameters of the system. An excellent agreement was found between the analytical model and the experimental FMR measurements. A general anisotropy diagram has been determined from the model, which defines the geometrical relation between the aspect ratio of both the magnetic and the nonmagnetic layers for which the effective anisotropy is zero. This diagram provides the values of the aspect ratio of the FM and the NM layers for which the easy axis is parallel or perpendicular to the cylinder axis. The diagram is general and valid for multilayered cylinders of any combination of FM and NM materials, within the validity of the considerations made, making it potentially useful for the design of multilayered nanowires with specific anisotropy properties.

ACKNOWLEDGMENTS

The authors thank R. Legras and E. Ferain for providing the polycarbonate membrane samples used in this study. J.D.L.T.M. thanks F. Elhoussine for her help and advice. This work was partly supported by the European Community's Sixth Framework Programme Contract No. NMP-CT-2004-505955 and the Interuniversity Attraction Poles Program (P6/42) Belgian State—Belgian Science Policy. A.E. thanks CONACyT for financial support through Grants No. 50650 and No. 48436.

[1] M. N. Baibich, J. M. Broto, A. Fert, F. Nguyen Van Dau, F. Petroff, P. Etienne, G. Creuzet, A. Friederich, and J. Chazelas, Phys. Rev. Lett. **61**, 2472 (1988).
[2] A. Fert and L. Piraux, J. Magn. Magn. Mater. **200**, 338 (1999).
[3] L. Piraux, J. M. George, J. F. Despres, C. Leroy, E. Ferain, R. Legras, K. Ounadjela, and A. Fert, Appl. Phys. Lett. **65**, 2484 (1994).
[4] A. Blondel, J. P. Meier, B. Boudin, and J. Ph Ansermet, Appl. Phys. Lett. **65**, 3019 (1994).
[5] K. Hong, J. Lee, J. Lee, Y.-D. Ko, J.-S. Chung, and J.-G. Kim, J. Magn. Magn. Mater. **304**, 60 (2006).
[6] L. Piraux, S. Dubois, and A. Fert, J. Magn. Magn. Mater. **159**, L287 (1996).
[7] K. Liu, K. Nagodawithana, P. C. Searson, and C. L. Chien, Phys. Rev. B **51**, 7381 (1995).
[8] X. T. Tang, G. C. Wang, and M. Shima, J. Appl. Phys. **99**, 033906 (2006).
[9] K. R. Pirota and M. Vazquez, Adv. Eng. Mater. **7**, 1111 (2005).

[10] L. W. Tan and B. J. H. Stadler, J. Mater. Res. **21**, 2870 (2006).
[11] S. Dubois, C. Marchal, J. M. Beuken, L. Piraux, J. L. Duvail, A. Fert, J. M. George, and J. L. Maurice, Appl. Phys. Lett. **70**, 396 (1997).
[12] S. Dubois, E. Chassaing, J. L. Duvail, L. Piraux, and M. G. Waals, J. Chim. Phys. Phys.-Chim. Biol. **96**, 1316 (1999).
[13] S. Valizadeh, L. Hultman, J. M. George, and P. Leisner, Adv. Funct. Mater. **12**, 766 (2002).
[14] K. Attenborough, R. Hart, S. J. Lane, M. Alper, and W. Schwarzacher, J. Magn. Magn. Mater. **148**, 335 (1995).
[15] X. T. Tang, G. C. Wang, and M. Shima, J. Appl. Phys. **99**, 123910 (2006).
[16] H. P. Liang, Y. G. Guo, J. S. Hu, C. F. Zhu, L. J. Wan, and C. L. Bai, Inorg. Chem. **44**, 3013 (2005).
[17] M. Chen, L. Sun, J. E. Bonevich, D. H. Reich, C. L. Chien, and P. C. Searson, Appl. Phys. Lett. **82**, 3310 (2003).
[18] A. Encinas, M. Lambert, and L. Piraux (unpublished).
[19] Y. K. Su, D. H. Qin, H. L. Zhang, H. Li, and H. L. Li, Chem. Phys. Lett. **388**, 406 (2004).
[20] Q. Huang, D. Davis, and E. J. Podlaha, J. Appl. Electrochem. **36**, 871 (2006).
[21] A. Bachtold, C. Terrier, M. Kruger, M. Henny, T. Hoss, C. Strunk, R. Huber, H. Birk, U. Staufer, and C. Schonenberger, Microelectron. Eng. **42**, 571 (1998).
[22] L. Vila, L. Piraux, J. M. George, A. Fert, and G. Faini, Appl. Phys. Lett. **80**, 3805 (2002).
[23] F. Elhoussine, L. Vila, L. Piraux, and G. Faini, J. Magn. Magn. Mater. **290**, 116 (2005).
[24] S. Fusil, L. Piraux, S. Mátéfi-Tempfli, S. Michotte, C. K. Saul, L. G. Pereira, K. Bozehouane, V. Cros, C. Deranlot, and G. M. George, Nanotechnology **16**, 2936 (2005).
[25] J. E. Wegrowe, D. Kelly, Y. Jaccard, P. Guittienne, and J. P. Ansermet, Europhys. Lett. **45**, 626 (1999).
[26] U. Ebels, A. Radulescu, Y. Henry, L. Piraux, and K. Ounadjela, Phys. Rev. Lett. **84**, 983 (2000).
[27] J. E. Wegrowe, A. Comment, Y. Jaccard, J. P. Ansermet, N. M. Dempsey, and J. P. Nozieres, Phys. Rev. B **61**, 12216 (2000).
[28] I. Enculescu, M. E. Toimil-Molares, C. Zet, M. Daub, L. Westerberg, R. Neumann, and R. Spohr, Appl. Phys. A: Mater. Sci. Process. **86**, 43 (2007).
[29] L. Gravier, S. Serrano-Guisan, F. Reuse, and J.-Ph. Ansermet, Phys. Rev. B **73**, 052410 (2006).
[30] X.-T. Tang, G. C. Wang, and M. Shima, J. Magn. Magn. Mater. **309**, 188 (2007).
[31] M. Darques, S. Michote, F. Elhoussine, A. Encinas, J. De la Torre Medina, and L. Piraux, J. Phys. D **39**, 5025 (2006).
[32] L. Sun, Y. Hao, C. L. Chien, and P. C. Searson, IBM J. Res. Dev. **49**, 79 (2005).
[33] M. Chen, C. L. Chien, and P. C. Searson, Chem. Mater. **18**, 1595 (2006).
[34] M. Chen, P. C. Searson, and C. L. Chien, J. Appl. Phys. **93**, 8253 (2003).
[35] E. Ferain and R. Legras, Nucl. Instrum. Methods Phys. Res. B **131**, 97 (1997), and references therein.
[36] A. Encinas-Oropesa, M. Demand, L. Piraux, I. Huynen, and U. Ebels, Phys. Rev. B **63**, 104415 (2001).
[37] M. Demand, A. Encinas-Oropesa, S. Kenane, U. Ebels, I. Huynen, and L. Piraux, J. Magn. Magn. Mater. **249**, 228 (2002).
[38] H. Zijlstra, *Experimental methods in magnetism* (North-Holland, Amsterdam, 1967), Vol. 2, p. 69.
[39] W. F. Brown, Jr. Am. J. Phys. **28**, 542 (1960).
[40] D. X. Chen, J. A. Brug, and R. B. Goldfarb, IEEE Trans. Magn. **27**, 3601 (1991).
[41] B. B. Pant, J. Appl. Phys. **79**, 6123 (1996).
[42] C. A. Ross, M. Hwang, M. Shima, H. I. Smith, M. Farhoud, T. A. Savas, W. Schwarzacher, J. Parrochon, W. Escoffier, H. N. Bertram, F. B. Humphrey, and M. Redjdal, J. Magn. Magn. Mater. **249**, 200 (2002).